A BRIEF HISTORY OF TRACEABLE GONIOPHOTOMETRY AT PTB

Maass, R., Lindemann, M., Sauter, G.

[1-3] Physikalisch-Technische Bundesanstalt, Braunschweig, Germany

Abstract

The Physikalisch-Technische Bundesanstalt (PTB) is the national metrology institute (NMI) of Germany and it focuses on the realization, maintenance and distribution of the SI units. Therefore, the determination of the luminous flux unit by goniophotometry has a long tradition. This paper gives an overview about the measurement systems developed, used and improved over more than 50 years in PTB. In the fifties and sixties of the past century a “single-lever-goniophotometer” was used to realize the unit *lumen* (lm) of luminous flux derived directly from the SI unit *candela* (cd) by luminous intensity transfer standard lamps. Later on, a large three frame gimbal mounted goniophotometer (radius 2500 mm) which allowed an automated movement of a photometer and simultaneously an additional tristimulus head around the measured lamp was used. For the measurement of small lamps and LEDs, a similar small three frame gimbal mounted goniophotometer (the so-called mini- goniophotometer) with a radius of only 300 mm was designed in the early 1980s. Compact goniophotometers especially for LED-measurements were also developed. In 2006, the first robot goniophotometer was installed in the new Albert Einstein Building of PTB.

1 Introduction

Luminous flux is economically the most important photometric quantity. It is necessary to derive its unit, *lumen,* directly from the SI base unit, *candela,* for luminous intensity. The fundamental realization of the luminous flux unit is by goniophotometry, even realization by the absolute integrating sphere method [1] needs - strictly analyzed - the relative luminous intensity distribution of the radiation of the lamp under test found by goniophotometric measurement.

The principle of goniophotometry is independent of the technical realizations of the different types of goniophotometers. A goniophotometer measures the illuminance $E(r,\vartheta,\varphi)$ on a closed envelope around a lamp measured with a $V(\lambda)$-matched photometer for all directions (ϑ,φ) of emission within the full solid angle ($4\pi\,\mathrm{sr}$) as shown in figure 1.

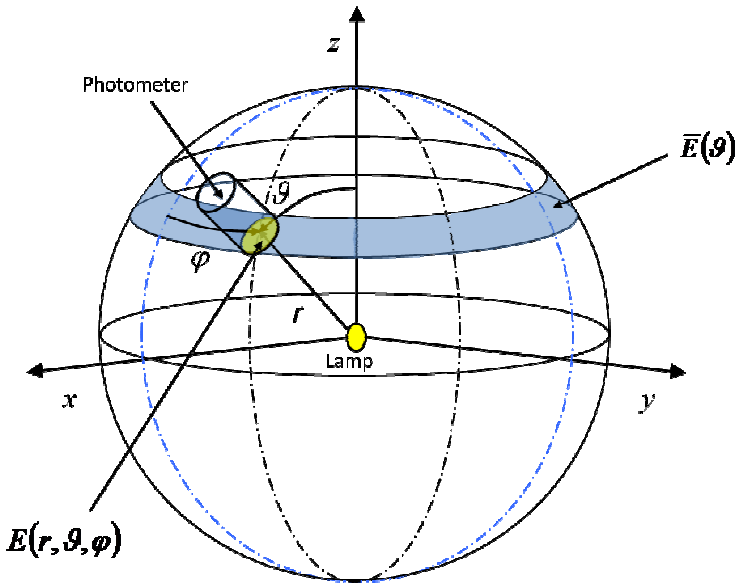

Figure 1. Illuminance E as a function of the radius vector $r(\vartheta,\varphi)$

Here the radius vector $r(\vartheta,\varphi)$ denotes the position of the photometer in sphere-coordinates and $r(\vartheta,\varphi)$ is always orthogonal to the entrance window (facing the lamp) of the photometer. The radius vector $r(\vartheta,\varphi)$ also describes the distance between the lamp and the photometer. The angle ϑ designates the photometer's position between the poles in a traditional way ($0 \le \vartheta \le \pi$). The angle φ designates the photometer's position in the equator direction ($0 \le \varphi \le 2\pi$). The luminous flux value Φ of the lamp can be calculated from the illuminance $E(\vartheta,\varphi)$, either from the luminous intensity definition $I = \mathrm{d}\Phi / \mathrm{d}\omega$ or from the definition of the illuminance $E = \mathrm{d}\Phi / \mathrm{d}A$.

$$\Phi = \int_{4\pi \mathrm{sr}} I(\vartheta,\varphi)\,\mathrm{d}\omega \tag{1}$$

$$\Phi = \int_{4\pi r^2} E(\vartheta,\varphi)\,\mathrm{d}A \tag{2}$$

The solid angle element $\mathrm{d}\omega$ of equation (1) is given by

$$\mathrm{d}\omega = \sin(\vartheta)\,\mathrm{d}\vartheta\,\mathrm{d}\varphi \tag{3}$$

and the area element $\mathrm{d}A$ of equation (2) is given by

$$\mathrm{d}A = r^2(\vartheta,\varphi)\sin(\vartheta)\,\mathrm{d}\vartheta\,\mathrm{d}\varphi\,. \tag{4}$$

The radius r of the radius vector $r(\vartheta,\varphi)$ can be treated as a constant value because usually it is not changed during the goniophotometric measurements. Then the luminous intensity distribution $I(\vartheta,\varphi)$ can be determined from the illuminance $E(\vartheta,\varphi)$ by the inverse square law.

$$I(\vartheta,\varphi) = r^2\, E(\vartheta,\kappa) \tag{5}$$

If the photometric distance r_L of the lamp under test is smaller than the measurement radius r of the goniophotometer then we can write equation (1) with equation (3) and $r = \text{const}$ as follows:

$$\Phi = r^2 \int_0^{2\pi} \mathrm{d}\varphi \int_0^{\pi} E(\vartheta,\varphi)\sin(\vartheta)\,\mathrm{d}\vartheta \tag{6}$$

On the other hand equation (2) with equation (4) and $r = \text{const}$ will lead to equation (6), as well. But we must keep in mind that for large lamps equation (5) might be wrong ($r_L > r$) but the luminous flux value according to equation (6) is right if the photometer evaluates the light correctly with the cosine of its incidence angle.

2 Goniophotometer Systems History at PTB

As already partially discussed in section 1, a suitable goniophotometer system for luminous flux measurements should meet the following main requirements:

1. Calibration via a luminous intensity lamp assuring traceability to the national realization of the unit *candela*
2. Relative movement between the lamp and the photometer with a rectangular intersection of the ϑ - and φ -axis
3. $V(\lambda)$-matched photometer (luminous flux)
4. Automatic data analysis
5. Independent measurement of the luminous flux value from the spatial distribution and the spectral distribution of the measured irradiance of light
6. Temperature independence of the photometer
7. Any burning position of the lamp under test
8. Air-conditioned environment
9. Small stray light section
10. Motor driven movement for the ϑ - and φ -axis
11. Tristimulus head (correlated colour temperature of luminous flux) and/or relative spectral distribution of the measured irradiance of light)
12. Measurement without movement of the lamp under test
13. Complete scan of illuminance/luminous intensity distribution of the lamp under test
14. Monitoring of lamp's output to correct for aging during the measurement
15. Temperature-conditioned walls (minimizes radiation exchange between discharge lamp and wall)
16. On-line stray light correction (especially for stray light tubes with greater field of view for measurements of large lamps like tubular fluorescent lamps)

17. Goniophotometer room luminaries should be shadowed during measurement
18. Variation of the measurement radius r (near field, far field measurements with imaging systems)

In goniophotometry we have to handle different coordinate systems. There are at least the lamp coordinate system, the room coordinate system and the goniophotometer coordinate system. Figure 1a shows these different coordinate systems with possible offsets and rotations between them.

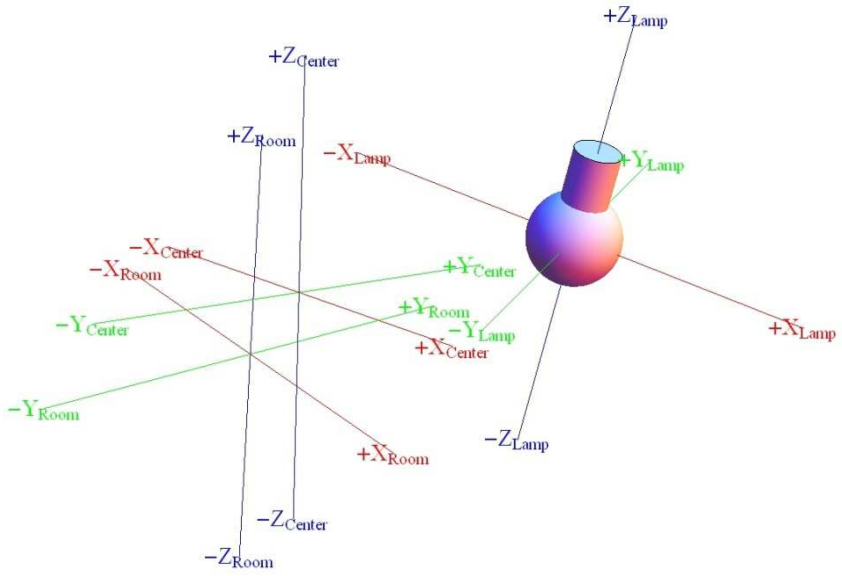

Figure 1a. Coordinate systems

Please note the goniophotometer coordinate system is called “Center” coordinate system in figure 1a. To simplify the further explanations we assume no offsets and rotations between the mentioned coordinate systems. That means the lamp coordinate system is equal the to the center coordinate system.

Next we will discuss the properties, advantages and disadvantages of different goniophotometer systems used at PTB over the decades and whether they meet the listed requirements or not. We will start in the fifties and sixties of the past century with a single lever goniophotometer and we will end with the state of the art robot goniophotometer, introduced in 2007.

2.1 Single Lever Goniophotometer (1950-1975)

In this time period a manually operated single lever goniophotometer as depicted in figure 2 was used. First in the fifties this instrument was equipped with a *visual* photometer. This photometer allowed the relative measurement of illuminance with an internally installed auxiliary lamp and reducer system [2, page 321]. The traceability to the national luminous intensity unit the *candela* was assured by the calibration of this visual photometer by luminous intensity transfer lamps (this complies with requirement 1) and according to distance measurements based on the national length unit the *meter*.

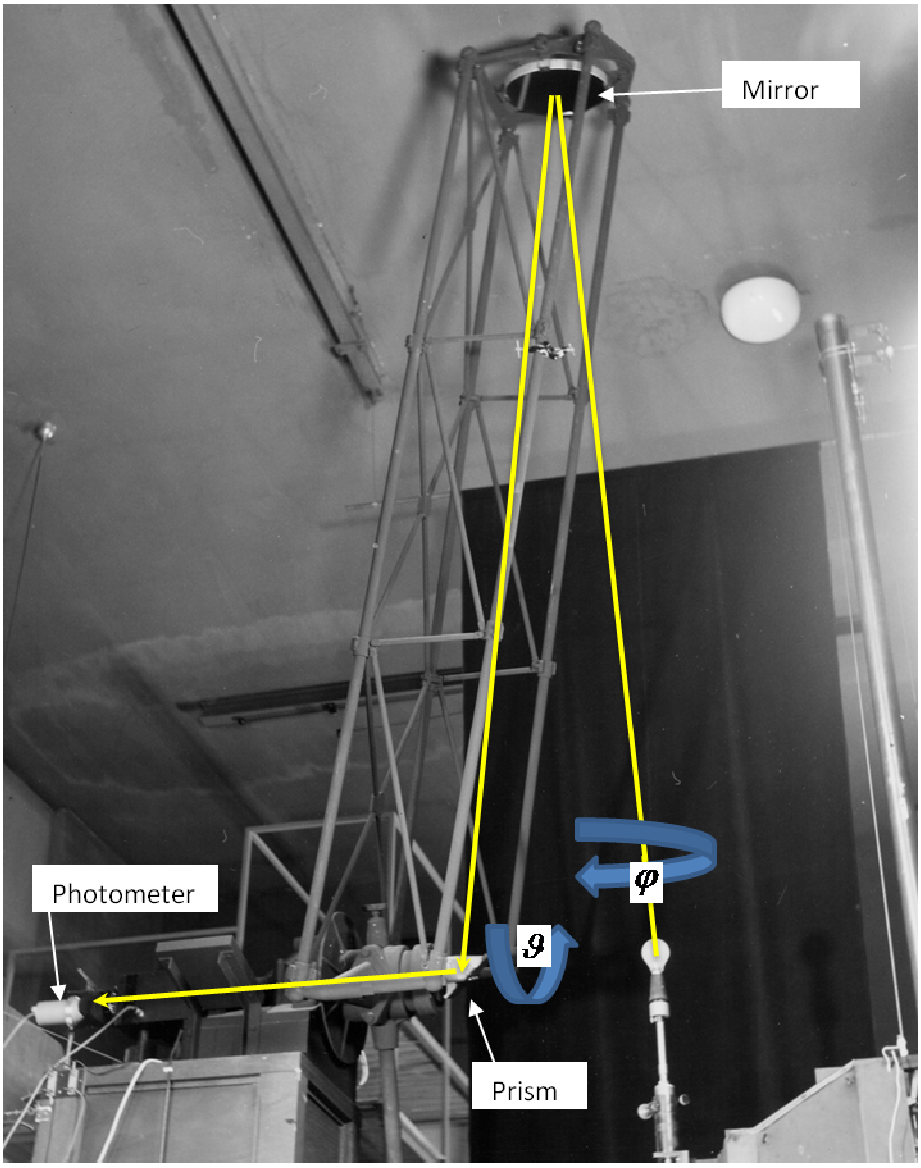

Figure 2. Single lever goniophotometer 1950-1975

Furthermore the *visual* photometer had to be installed at a fixed place as shown in figure 2 due to the position dependency of the auxiliary lamp inside the photometer. Hence a mirror/prism system was used to redirect the light from the lamp under test to the *visual* photometer. More detailed information about a system like this can be found here [2, p. 319]. This arrangement complies with requirement 2.

For a complete luminous flux measurement a number illuminance values for manually adjusted different sphere-coordinates (ϑ,φ) has to be measured. If the fictive sphere of figure 1 is divided into parallel zones in the ϑ-direction and each zone i is divided into n sections of equal length with an illuminance of E_j, it is possible to calculate the mean illuminance $\overline{E_i}$ of each zone i by

$$\overline{E_i} = \frac{1}{n}\sum_{j=1}^{n} E_{i,j} \tag{7}$$

and the luminous flux value by numerical integration with equation (8).

$$\Phi = 2\pi r^2 \sum_{i=0}^{m-1} \left(\cos(\vartheta_i) - \cos(\vartheta_{i+1})\right)\overline{E_i} \tag{8}$$

The total number of single illuminance measurements depends on the spatial distribution of light of the lamp under test. Due to the manual adjustment of the large lever (ϑ) and turning the lamp (φ) as well as the adjustment of the photometer, this method was very time-consuming. For example; let us assume 600 points to be measured (from today's viewpoint not a great many) and let us say 25 seconds per point. It took more than four hours to measure a lamp with a relative homogenous spatial distribution.

In 1963 an international comparison of the luminous flux unit of discharge lamps without fluorescent material was carried out. These lamps had a very inhomogeneous spatial distribution of light. So it was impossible to measure these lamps with the described method because the number of measuring points needed would have been much too large. The solution as described in [3] was to replace the *visual* photometer by a rough $V(\lambda)$-matched photomultiplier, adding an electrical drive to the φ-axis and a high precision capacitor for integrating the photocurrent of the photomultiplier. Then for each ϑ-adjustment of the large lever the drive of the φ-axis rotated the lamp with constant velocity while the precision capacitor was integrating the photocurrent of the photomultiplier. After about $t = 5\,\text{minutes}$ for one turn in the φ-direction, the charge $Q = C \cdot U$ of the precision capacitor represented the mean illuminance

$$\overline{E_i} = k \cdot C \frac{U}{t} \tag{9}$$

of a measured zone i. Again we get the luminous flux value from equation (8). There is no need to know the value of kC because it has been eliminated during the calibration process with a known illuminance from a luminous intensity lamp but it must be constant over the total measurement time. Later on, in the sixties, the visual photometer was also replaced by a modern $V(\lambda)$-matched photometer based on filtered silicon photodiodes in combination with a photocurrent to voltage converter and an x/y-plotter to plot the illuminance distribution of a zone. Then the mean illuminance was determined in a graphical integration or a numerical integration way.

We will see in the next sections that this method of “analogue zone integration” is very similar to the digital evaluation performed in goniophotometers, today.

These last two improvements met the requirement 3 and partially complied with requirement 4.

2.2 Gimbal Mounted Goniophotometer (1976-2007)

The existing single lever goniophotometer really needs a “helping hand” to move it manually from point to point. The computation of the luminous flux value was carried out “by hand”, too. This procedure needed a long time and was together with additional requirements for the measurement of large tubular fluorescent lamps, micro lamps and of course LEDs basically the reason to introduce a new goniophotometer.

2.2.1 Large Gimbal Mounted Goniophotometer

Figure 3. Large gimbal mounted goniophotometer 1976-2007

After intensively rebuilding several rooms of the Kösters Building, it was possible to assemble the newly constructed large gimbal mounted goniophotometer [4] in the new goniophotometer room of approx. 7 to 10 to 8 m^3. Figure 3 shows a photograph of the large gimbal mounted goniophotometer. It also shows a tubular fluorescent lamp under test.

This room was also equipped with additional regulated electrical room heating to adjust the air temperature according to the required measurement conditions. In principle a gimbal mounted goniophotometer as in figure 4 consists of three frames where the outer frame allows any spatial orientation of the lamp under test by turning this so-called α-frame around the y-axis. Inside this outer α-frame the φ-frame is pivot-mounted which provides an endless variety of ways of turning this frame around the z-axis. Finally there is the ϑ-frame which is also pivot-mounted inside the φ-frame but the working range of this last frame is limited to a half turn. All three frames are mechanically balanced and motor driven. Their speed was manually adjustable by 10-turn precision potentiometers because the frame speed regulation was of an analogue type. The angle determination for all frames was done by 13-bit angle encoders. The photometer was attached to the ϑ-frame (see figure 4) which gave a fixed measurement radius of 2500 mm. It was possible to attach a second photometer or a tristimulus head at the opposite end of the same ϑ-frame. In this case the working range was limited to $4° \le \vartheta \le 176°$ by the two lamp holder rods which were very suitable for the measurement of tubular fluorescent lamps. In case of single socket lamps one photometer was detached and the crank of this frame side

was turned to the give clearance to the lamp holder rod. This allowed a working range of $0° \leq \vartheta \leq 176°$.

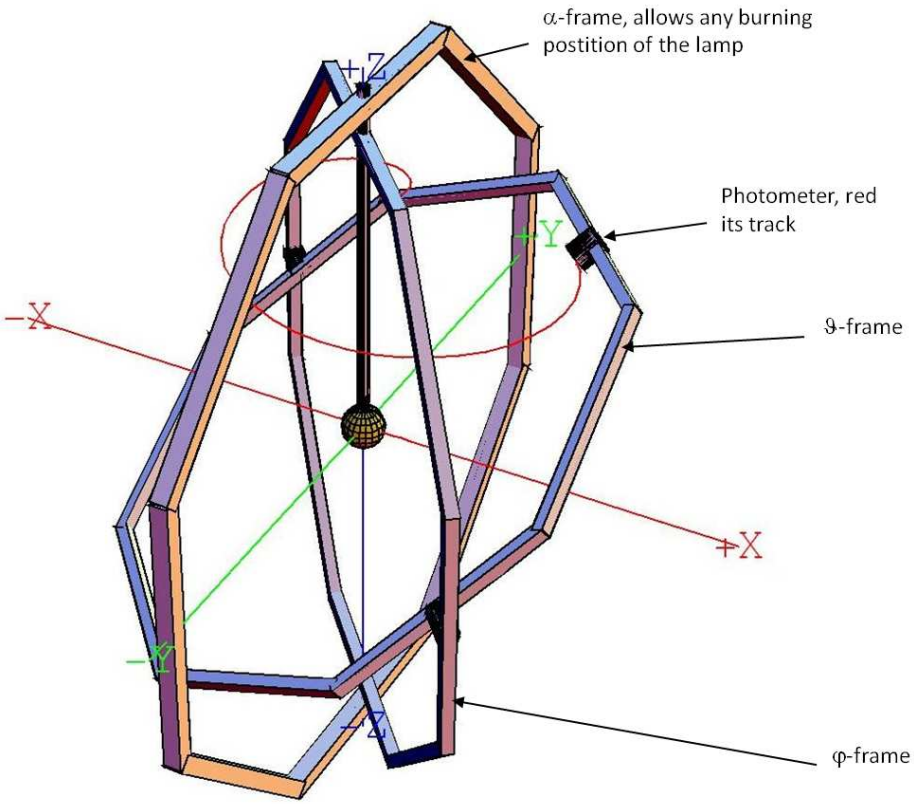

Figure 4. Large gimbal mounted goniophotometer 1976-2007

According to equation (6) we have to integrate the measured illuminance over the full solid angle of $4\pi\,\mathrm{sr}$ to get the luminous flux value. So it is obvious to use a digital time integrating method to collect and store measured illuminance values. Figure 5 shows the signal flow. The photometer and/or tristimulus head as well as the photocurrent-to-voltage converter including the voltage-to-frequency converter were of a temperature regulated type, too.

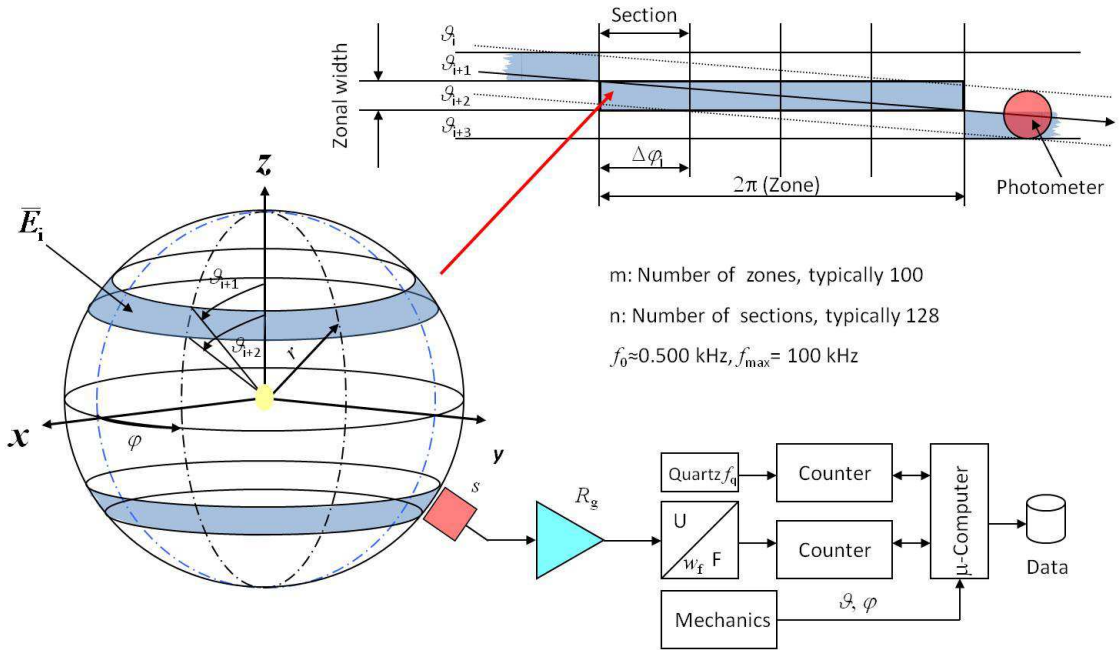

Figure 5. Signal flow

The photocurrent from the photometer with the luminous responsivity s normalized to CIE illuminant A is converted with R_g in a voltage U and further converted in a frequency f with the related conversion factor w_f. This frequency is counted by a digital counter as the signal. The quartz frequency f_q is counted simultaneously by a second counter to get the measured signal frequency back during the data analysis. This method assures the above-mentioned signal/time integration. As already stated the fictive sphere around the lamp under test is divided into zones and sections (see figure 5, upper part). Due to the analogue speed regulation of the two moving frames, positive and negative acceleration phases at the beginning and ending of a full scan and load alternation of the rotating system, a small wow and flutter is unavoidable. $\Delta\varphi_j$, the section length, reduced this influence. With this weighting the mean illuminance $\overline{E}_i$ is computable with equation (10)

$$\overline{E}_i = \frac{1}{2\pi\cdot\left(s\cdot w_f\cdot R_g\right)}\cdot\sum_{j=1}^{n}\Delta\varphi_j\cdot\left(f_q\frac{\Delta y_{i,j}}{\Delta t_{i,j}}-f_0\right) \qquad (10)$$

where f_0 is the dark frequency (shadowed photometer) and $\Delta y_{i,j}$ are the difference signal counts and $\Delta t_{i,j}$ difference time counts with respect to the section start and end. Again the luminous flux value is determined by equation (8), but we have to add corrections for stray light c_{str}, the spectral mismatch of the photometer c_{spec} and deviations from the stated electrical measuring conditions c_{elec} as described in equation (11)

$$\Phi = c_{str}\cdot c_{spec}\cdot c_{elec}\cdot 2\pi r^2\cdot\sum_{i=0}^{m-1}\left(\cos\vartheta_i-\cos\vartheta_{i+1}\right)\cdot\overline{E}_i \qquad (11)$$

During a measurement the walls of the goniophotometer room are also illuminated by the lamp under test as well as the goniophotometer itself. This illumination is also seen by the photometer attached to the goniophotometer and leads to a stray light illumination on the sensitive area of the photometer. This stray light illumination also depends on the field of view of the photometer given by the stray light reduction tube in front of the photometer. That means the stray light correction factor c_{str} has to be determined for any used stray light reduction tube with its specific field of view. This was carried out by different baffles of different diameters which were positioned between the lamp and the photometer during a normal luminous flux measurement. A detailed description of the method can be found here [5].

The technical realization of a photometer is always an approximation to $V(\lambda)$, only. That means in most cases a correction of this mismatch has to be applied. Generally for all kinds of lamps with a relative spectral power distribution $S(\lambda)$ the correction factor is obtained from equation (12)

$$c_{\mathrm{spek}} = \frac{\int V(\lambda)\cdot S(\lambda)\,\mathrm{d}\lambda}{\int s_{\mathrm{rel}}(\lambda)\cdot S(\lambda)\,\mathrm{d}\lambda} \Bigg/ \frac{\int V(\lambda)\cdot P(\lambda,T_{\mathrm{A}})\,\mathrm{d}\lambda}{\int s_{\mathrm{rel}}(\lambda)\cdot P(\lambda,T_{\mathrm{A}})\,\mathrm{d}\lambda} \tag{12}$$

However, we have to know the relative spectral responsivity $s_{\mathrm{rel}}(\lambda)$ of the photometer. $P(\lambda,T_{\mathrm{A}})$ indicates a Planckian radiator at a distribution temperature of $T_{\mathrm{A}} = 2856\ \mathrm{K}$. In case of tungsten lamps there is a more simple way without knowing $s_{\mathrm{rel}}(\lambda)$ to correct for a spectral mismatch according to equation (13). Where $E(T)$ is the corrected illuminance for a distribution temperature T from

$$E(T) = \frac{y(T)}{s}\left(\frac{T}{T_{\mathrm{A}}}\right)^{m_y} \tag{13}$$

a measured photocurrent $y(T)$ and a luminous responsivtiy s of the photometer for CIE illuminant A. A property of the photometer is the exponent m_y. The index "y" indicates an exponent for a $V(\lambda)$-matched photometer or the y-channel of a tristimulus head. The other channels will have different exponents. If this value of m_y is close to zero, for example m_y=0.018, the photometer's match is of good quality. The exponent m_y (and the others) can be found from a fit of known pairs of $(E(T), T)$ from a luminous intensity lamp at different working points as described here [6, 7]. Finally the correction factor for tungsten lamps can be written as follows

$$c_{\mathrm{spec}} = \left(\frac{T}{T_{\mathrm{A}}}\right)^{m_y} \tag{14}$$

Also in case of tungsten lamps operated close to CIE illuminant A the determination of c_{elec} is easy because the value of luminous flux is a function of the electrical operating current J and we can use the following equation (15) to find c_{elec}

$$c_{\mathrm{elec}} = \left(\frac{J}{J_0}\right)^{-m_J} \tag{15}$$

where J_0 is the nominal current and $m_J \cong 6.84$. More information can be found here [7].

The data analysis for the tristimulus head was carried out in the same way to get the chromaticity (x, y) of the luminous flux from the three channels of the tristimulus head

$$x = \frac{\Phi_X}{\Phi_X + \Phi_Y + \Phi_Z} \tag{16}$$

$$y = \frac{\Phi_Y}{\Phi_X + \Phi_Y + \Phi_Z} \tag{17}$$

Unfortunately, only the total luminous flux value with the related chromaticity of the source could be determined, the spatial information was lost due to poor computer performance. In 1991 however, all computers, analogue systems, wiring and further parts were replaced by modern equipment. From that time on all the spatial data were stored in suitable media. As long ago as in the year 1997 this gimbal mounted goniophotometer was equipped additionally with an array spectrometer to measure the relative power distribution of the radiation synchronized to the luminous flux measurement. But the photometer and the input optic of the array spectrometer had different fields of view and slightly different positions on the goniophotometer system which complicated the final data analysis. However, now it was possible to get spatial spectra information of lamps under test.

In its last version from 1997 this goniophotometer met the requirements 1-14 from the list at the beginning of section 2. The relative expanded $k = 2$ measurement uncertainty for luminous flux values of standard lamps was 0.60 %.

2.2.2 Small Gimbal Mounted Goniophotometer

For the measurement of small lamps and LEDs a similar three frame gimbal mounted goniophotometer with a radius of only 300 mm was designed in the early 1980s. The photograph in figure 6 shows this so-called “mini-goniophotometer”.

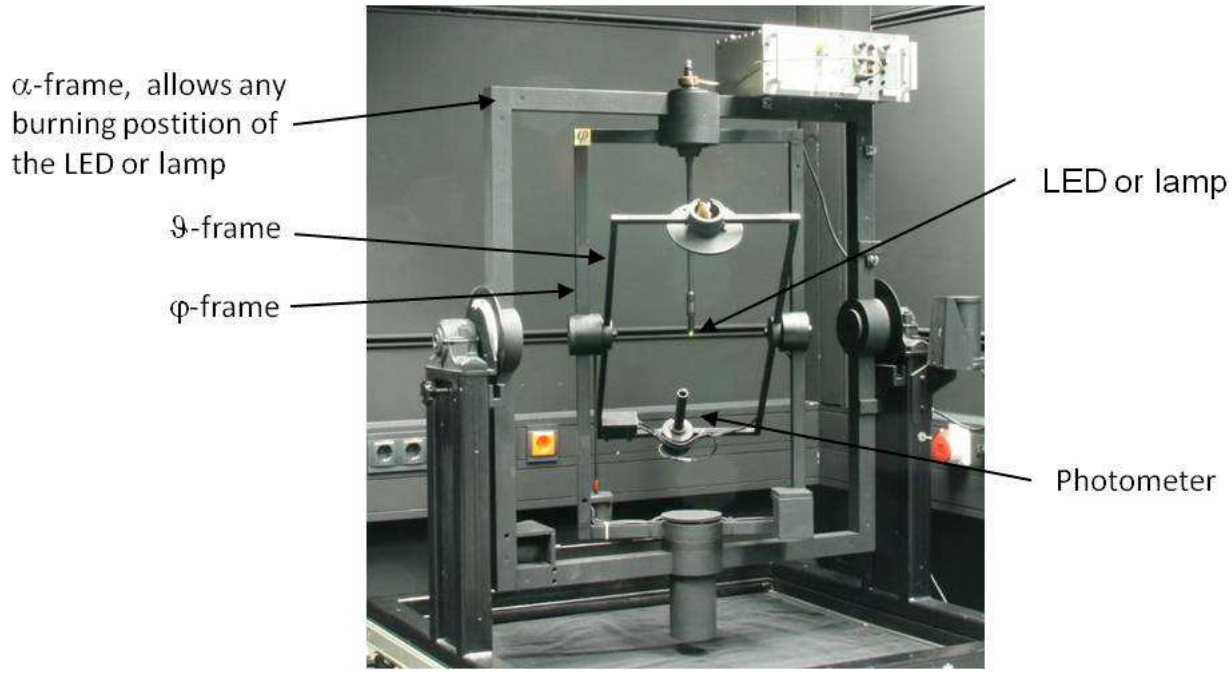

Figure 6. Small gimbal mounted goniophotometer 1982-2007

The theory of operation was exactly the same as the large gimbal mounted goniophotometer. Also the signal flow including voltage-to-frequency converters and counters was the same. All aspects of this system have thus already been discussed under section 2.2.1. In 2007 this instrument was replaced by a goniophotometer especially designed for measurements of LEDs [10].

2.3 Robot Goniophotometer (2006 ...)

At the end of the nineties the planning of a new type of goniophotometer became more and more concrete, because PTB decided to construct a new building for the optics division, which is now called Albert Einstein-Building. So in principle this new building was designed “around” the new robot-goniophotometer. As for back as in 1995/1996 G. Sauter showed that goniophotometry by robots

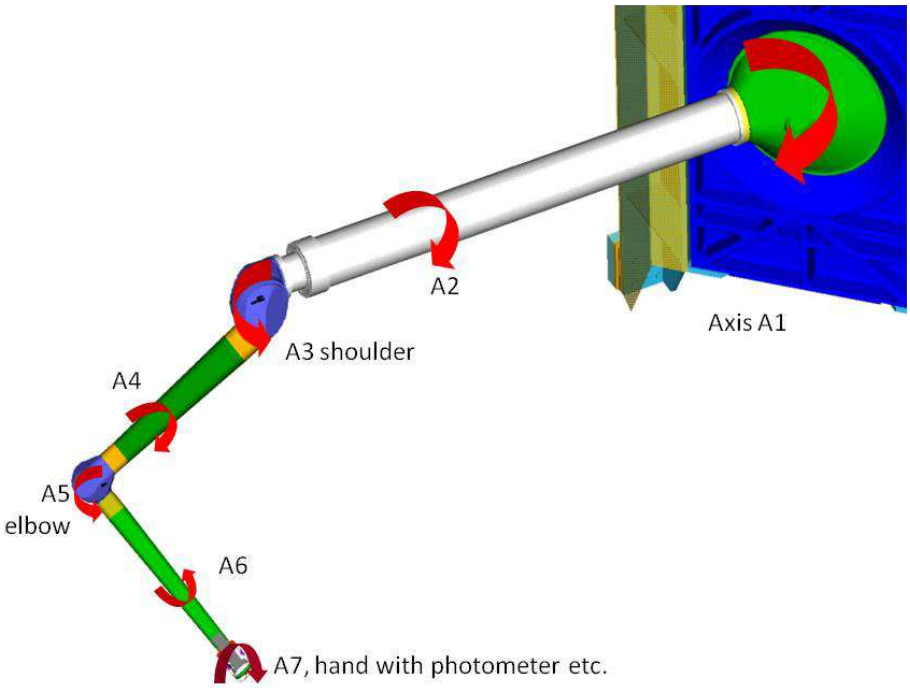

Figure 7. Arm of robot goniophotometer

is possible and has an advantage compared to a gimbal mounted system [8]. As also described in [8] so-called service robots are suitable to realize a robot goniophotometer. Their design is slim with long arms and they are of light weight construction to move photometers and hold lamps. They also have a high flexibility to move the photometer(s) on desired tracks with different radii ($1000\text{mm} \le r \le 3000\text{mm}$) over the fictitious surface of a sphere around the lamp. Each robot is of seven degree of freedom (DOF) type which guarantees the required flexibility and range of operation (see figure 7). In fact the robot goniophotometer consists of two robots to cover the whole solid angle of $4\pi\,\text{sr}$ and one similar robot to position the lamp under test in the goniophotometer room. All robot supports were directly attached to the building’s concrete to assure the long term stability of their spatial position. Figure 8 shows the goniophotometer room with robots measuring an LED-traffic light.

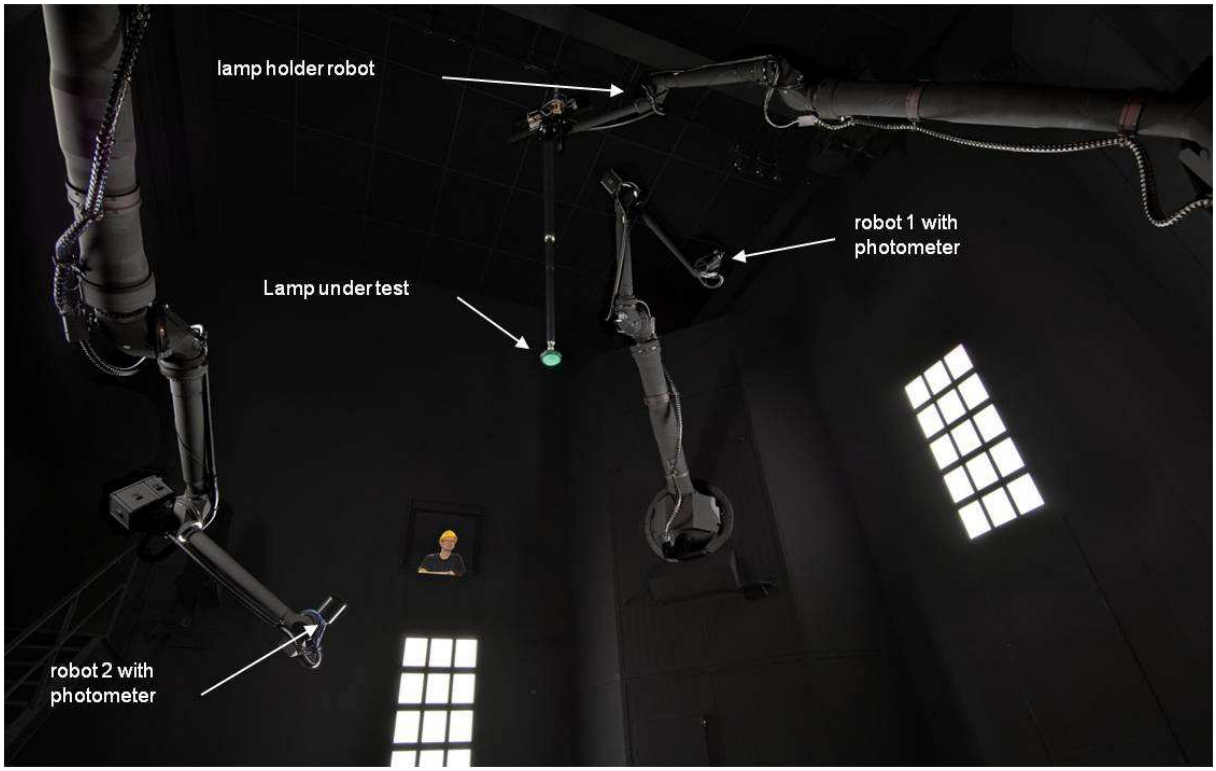

Figure 8. Robot goniophotometer 2006...

In contrast to a gimbal mounted goniophotometer the measurement radius is variable by turning all the seven axes into appropriate positions. Due to the large redundancy of a seven DOF robot, the target position/orientation of the photometer is reachable with many different positions of the seven axes. Hence we need a strategy to find positions of the axes. That means in our case to find the axes positions in such a way, that the distances of all other parts of the robot from the centre are maximized. Special software is used to calculate all seven angles of the axes expressed in counts of each axes' angle encoder from the desired spherical coordinates (r, ϑ, φ). During the measurement of a lamp the robot's control system reads these seven angles (counts) from a given list every 10 ms and tries to adjust each axis according to this value. After the adjusting process all seven angles are read synchronously and stored in a database with the related photometric data. In principle the photometric signal flow is very similar to the large gimbal mounted goniophotometer as described in section 2.2.1. But there is one additional feature, because we have a distributed data acquisition system, it is necessary to use a time stamp of the same clock (1 MHz) for all systems to synchronize the data later during the analysis process.

As the described setting of each axis is the result of a regulation process, the actual value will differ from the desired angle. Therefore we have to recalculate the actual positions/orientation of the photometer from the actual axes' angles.

It is common in robotics to describe a (rigid) robot like a mechanical chain with so-called Denavit-Hartenberg Parameters (Later called DH parameters), see [9]. Table 1 shows the DH parameters of one robot 1 as an example.

Table 1. DH parameters of robot 1

axis i	$\Delta\theta_i$ offset to rotation around Z-axis	α_i rotation around X-axis	d_i translation in Z-axis	a_i translation in X-axis
1	-1.438°	45.024°	0.000 mm	-0.400 mm
2	191.088°	-90.026°	2686.322 mm	0.696 mm
3	178.585°	89.996°	274.088 mm	0.781 mm
4	6.229°	-90.022°	1410.499 mm	0.474 mm
5	-0.141°	-89.955°	173.036 mm	-0.779 mm
6	-0.924°	90.032°	1191.007 mm	0.223 mm
7	180.443°	90.007°	91.130 mm	0.000 mm

With these parameters and the actual angle θ_i for each axis, it is possible to calculate the position/orientation of the 7th axis relative to the robot's base frame. With 7 matrix equations of type (18) the position(marked blue)/orientation(marked green) of each axis is calculable.

$$T_i = \begin{pmatrix} \cos(\Delta\theta_i+\theta_i) & -\sin(\Delta\theta_i+\theta_i)\cos\alpha_i & \sin(\Delta\theta_i+\theta_i)\sin\alpha_i & a_i\cos(\Delta\theta_i+\theta_i) \\ \sin(\Delta\theta_i+\theta_i) & \cos(\Delta\theta_i+\theta_i)\cos\alpha_i & -\cos(\Delta\theta_i+\theta_i)\sin\alpha_i & a_i\sin(\Delta\theta_i+\theta_i) \\ 0 & \sin\alpha_i & \cos\alpha_i & d_i \\ 0 & 0 & 0 & 1 \end{pmatrix} \quad (18)$$

So the position/orientation of axis 7 relative to the base frame of the robot is the vector product $T_1 \bullet T_2 \bullet T_3 \bullet T_4 \bullet T_5 \bullet T_6 \bullet T_7$. But we are interested in the position/orientation of the photometer in relation to the centre of a fictitious sphere. For this we have to know the position/orientation of the robot's base frame to the centre coordinate system and the photometer in relation to axis 7. This is simply done by adding a base frame matrix F and a tool matrix W. Both are of the same style as equation (18). Then we have the position and orientation of the photometer P^* with equation (19).

$$P^* = F \bullet T_1 \bullet T_2 \bullet T_3 \bullet T_4 \bullet T_5 \bullet T_6 \bullet T_7 \bullet W \quad (19)$$

Figure 9 shows all the robot's joints with their own coordinate systems (1..7) as well as the base frame and tool (=photometer) coordinate systems in a schematic way. P^* is referenced to the centre coordinate systems. Additionally a typically track of the photometer is shown. Due to the lamp holder stick (not shown here) at the upper equator region, the tracks are compressed to avoid a collision with this lamp holder stick.

As already mentioned, equation (19) is valid only for a rigid robot. In practice the robot's orientation/position P^* is influenced by static gravity forces and dynamic forces during the movement which causes bending of the robot's structure as well as by changing of the structure length caused by temperature differences to the reference temperature. Thus, we have to add a correction term to equation (19) like the following:

$$P = C\left(\theta_1.....\theta_7, \frac{\mathrm{d}\theta_1}{\mathrm{d}t}.....\frac{\mathrm{d}\theta_7}{\mathrm{d}t}, T_{\mathrm{amb}}, R\right) \bullet F \bullet T_1 \bullet T_2 \bullet T_3 \bullet T_4 \bullet T_5 \bullet T_6 \bullet T_7 \bullet W \tag{20}$$

where $C\left(\theta_1.....\theta_7, \frac{\mathrm{d}\theta_1}{\mathrm{d}t}.....\frac{\mathrm{d}\theta_7}{\mathrm{d}t}, T_{\mathrm{amb}}, R\right)$ describes the final correction based on the angles $\theta_1.....\theta_7$ of all axes, their time derivates $\frac{\mathrm{d}\theta_1}{\mathrm{d}t}.....\frac{\mathrm{d}\theta_7}{\mathrm{d}t}$ and the environment's temperature T_{amb}.

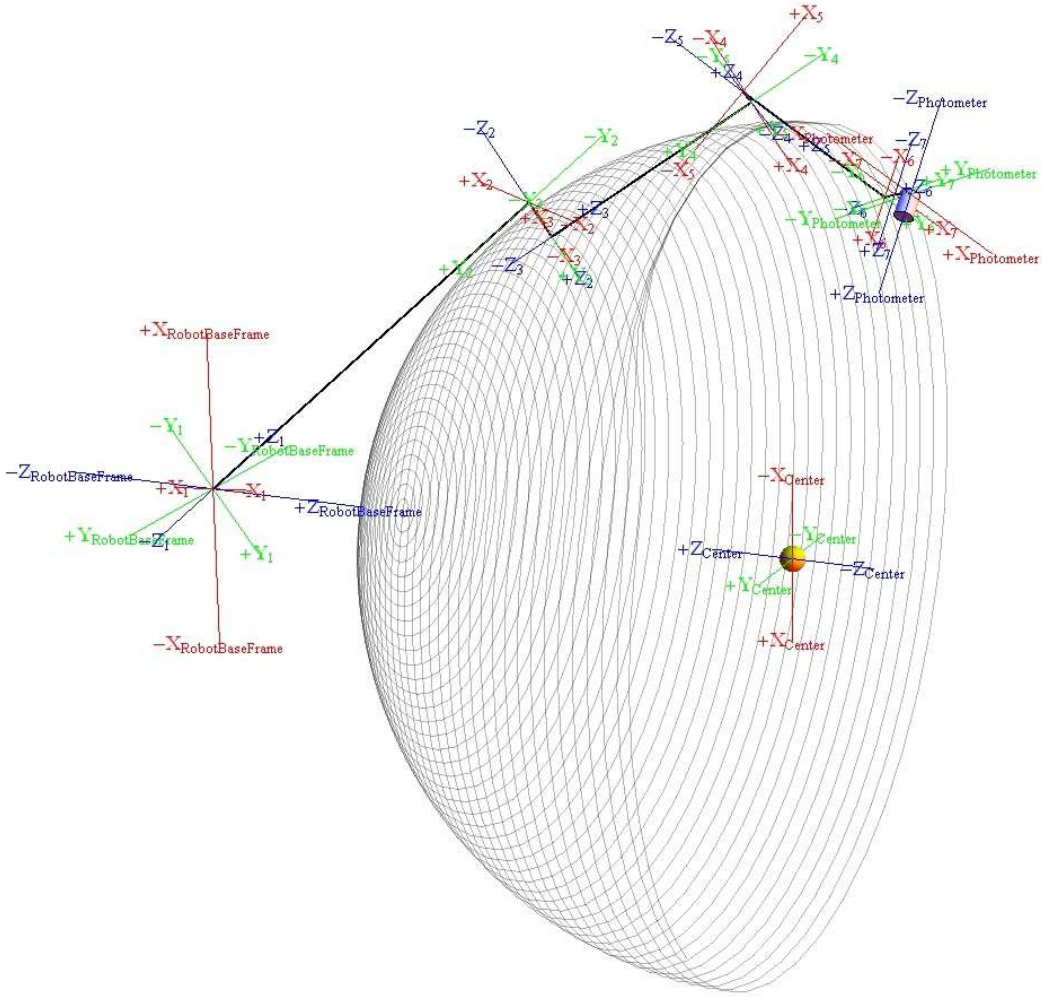

Figure 9. Coordinate systems of robot goniophotometer and sample track

The parameter R stands for a large data set to describe the robot's properties like the dimensions of the robot, mass distribution and so on. The computation of $C(\ )$ is complicated and was created by the robot's manufacturer. Due to competition on the robot market, $C(\ )$ must be treated as confidential and cannot be published. But the effect of $C(\ )$ is publishable. Figure 10 shows this effect.

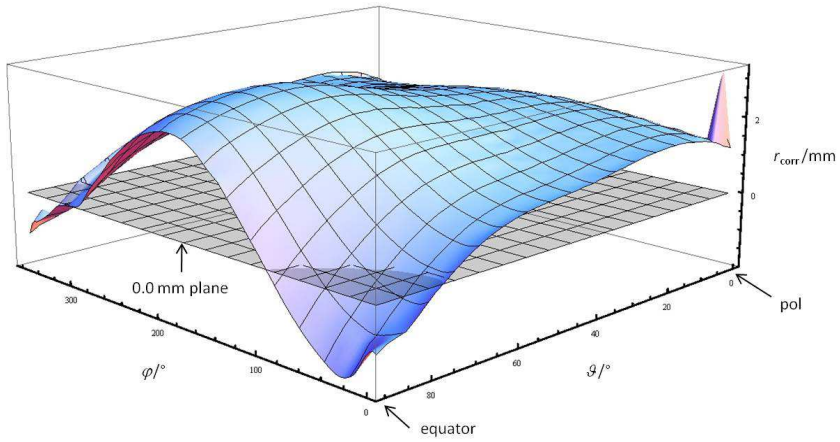

Figure 10. Effect of radius correction

The correction range reaches from approx. $-2\,\mathrm{mm} < r < 3\,\mathrm{mm}$ depending on the photometer's (ϑ,φ) position. The equator area needs more correction than the polar area due to larger centrifugal forces. From the position part of P the current radius r is obtained. Since the data flow is nearly the same as in shown in figure 5, the determination of the luminous flux value is in principle the same as using equation (11) with equation (10), but due to two photometers we have to do this separately for both robots. Equations (21) and (22) are examples of robot 1. Please note, that the current radius $r_{1,i}$ is within the sum of equation (22). The goniophotometer is also equipped with a monitoring photometer. This photometer is not moved during the measurement but is always pointed from a fixed point to the lamp under test which allows a correction for a possible aging of the lamp during the measurement process as a function of time ($c_{\mathrm{mon}}(t_{1,i})$).

$$\overline{E}_{1,i} = \frac{1}{2\pi\left(s_1\, w_{1,\mathrm{f}}\, R_{1,\mathrm{g}}\right)} \cdot \sum_{j=1}^{n_1} \Delta\varphi_{1,j} \left(f_{\mathrm{q}} \frac{\Delta y_{1,i,j}}{\Delta t_{1,i,j}} - f_{1,0} \right) \tag{21}$$

$$\Phi_1 = c_{1,\mathrm{str}} \cdot c_{1,\mathrm{spec}} \cdot 2\pi \cdot \sum_{i=0}^{m_1-1} r_{1,i}^2 \cdot c_{\mathrm{mon}}\left(t_{1,i}\right) \cdot \left(\cos\vartheta_{1,i} - \cos\vartheta_{1,i+1}\right) \cdot \overline{E}_{1,i} \tag{22}$$

Similar equations are valid for the data of robot 2 and so the luminous flux is the sum of Φ_1 and Φ_2 corrected with the factor c_{elec} from equation (15).

$$\Phi = c_{\mathrm{elec}} \cdot \left(\Phi_1 + \Phi_2\right) \tag{23}$$

The determination of the stray light correction c_{str} in the robot goniophotometer room is different from the method used for the gimbal mounted goniophotometer: It is difficult to mount baffles between the photometer and the lamp as described in [5]. Here we calculate the correction c_{str} directly from the luminance distribution of the walls of the goniophotometer room. With the knowledge of the geometrical and photometric properties of the room, the luminous intensity distribution of the lamp and the correction could be calculated. Here the effect of the reflected light on the walls

and the arms of the robots is measured by an additional so-called “back-looking photometer” as described in [11].

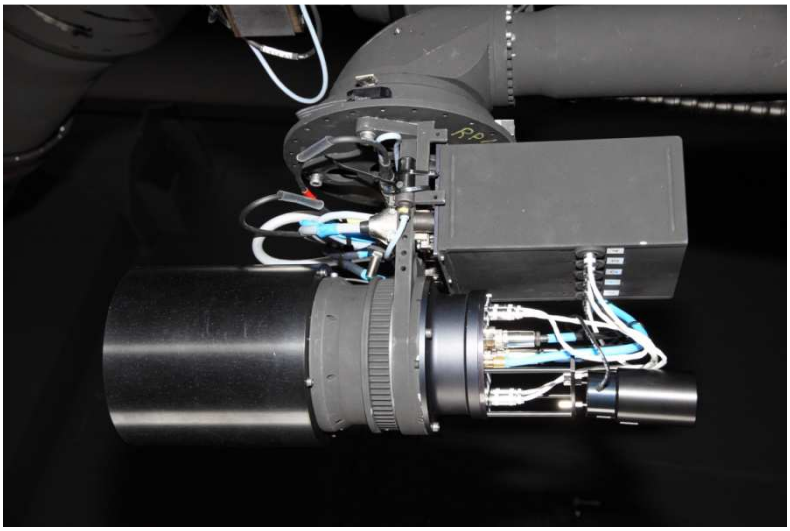

Figure 11. Photometer (on the left) and Back-Looking-Photometer (on the right)

Figure 11 shows a photograph of a robots “hand” with the photometer and back-looking photometer. The back-looking photometer is a little bit tilted. Otherwise the measured illuminance is influenced by the shadow of the photometer on the wall.

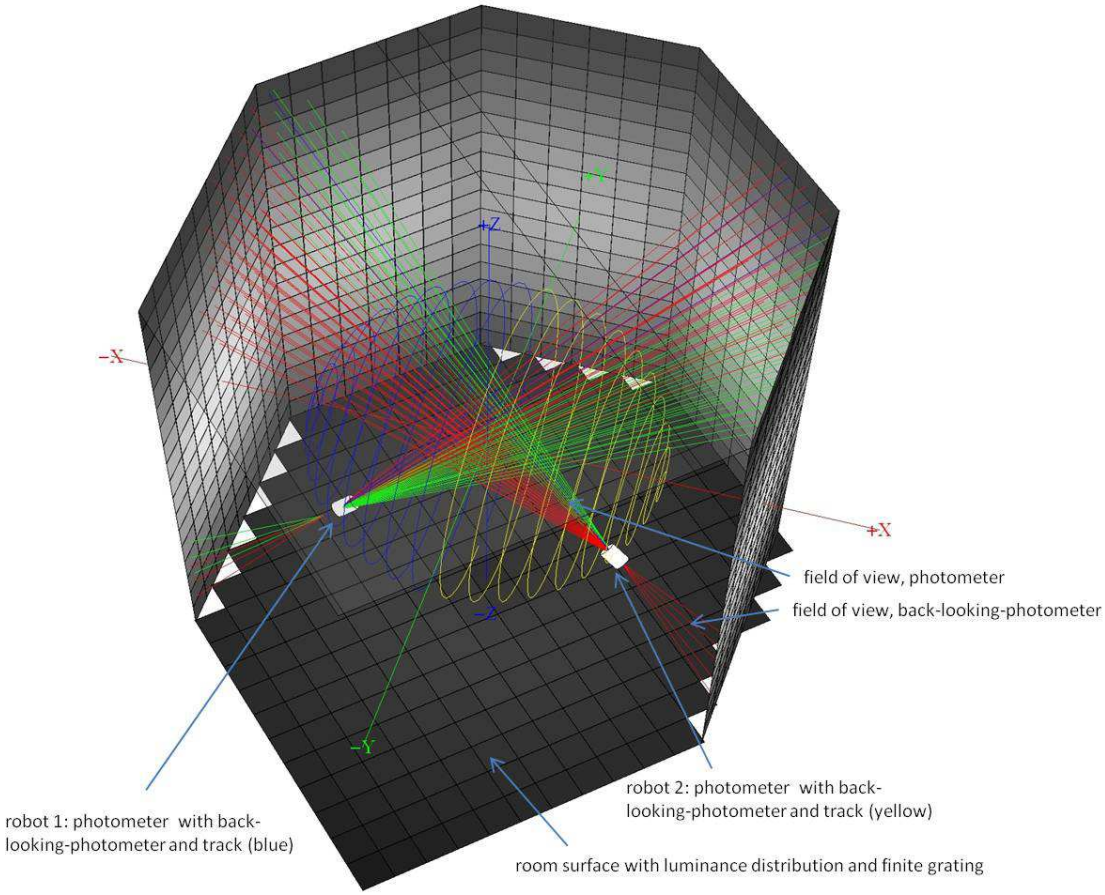

Figure 12. Measurement and effect of stray light

Figure 12 shows a sample stray light situation of the goniophotometer room with finite element grating of the luminance caused by the lamp under test. This example works with finite squares of 0.5 m x 0.5 m to make the grating visible. In reality smaller squares of 0.1 m x 0.1 m are used. Of course the effect of stray light on the photometer's active area depends on the field of view of the used stray light tube in front of the photometer. Currently there are two types of stray light tubes in use with fields of view from approx. 15° up to 22.5°. Their typical correction factors are 0.9995 and 0.9990. Each photometer is equipped with a back-looking stray light photometer to determined the luminance distribution with its own field of view. Note that each back-looking photometer will measure the luminance distribution used as a correction for the opposite photometer. Now it is possible to calculate the luminous flux value and related standard measurement uncertainty. Table 2 illustrates the results from a simplified Monte Carlo simulation (MC) of the calibration of an OSRAM Wi 4 luminous flux standard lamp. The spatial luminous intensity distribution is shown in figure 13.

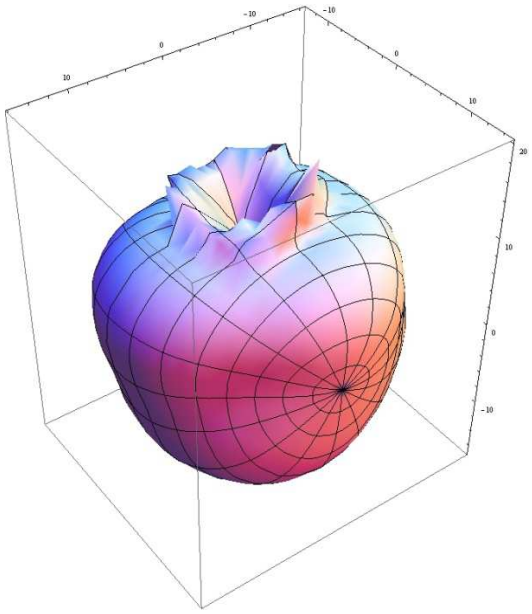

Figure 13. Spatial luminous intensity distribution of OSRAM Wi4

The MC is based on the following equation (24) and detailed values are shown in table 2.

$$\Phi = c_{\mathrm{str}} \cdot \left(\frac{J}{J_0}\right)^{-m_j} \cdot \left(\begin{array}{l} \left(\frac{T}{T_{\mathrm{A}}}\right)^{m_{1,y}} \sum_{\mathrm{i}=0}^{m_1-1} (\Delta r + r_{1,i})^2 \cdot c_{\mathrm{cm}} \cdot c_{\mathrm{mon}}\left(t_{1,i}\right) \cdot \left(\cos\vartheta_{1,i} - \cos\vartheta_{1,i+1}\right) \cdot \frac{\sum_{j=1}^{n_1} \Delta\varphi_{1,j} \cdot \left(c_{\mathrm{FH}} \cdot F_{1,i,j} - c_{\mathrm{FD}} \cdot f_{1,0}\right)}{s_1 \cdot w_{1,f} \cdot R_{1,g}} + \\ \left(\frac{T}{T_{\mathrm{A}}}\right)^{m_{2,y}} \sum_{i=0}^{m_2-1} (\Delta r + r_{2,i})^2 \cdot c_{\mathrm{cm}} \cdot c_{\mathrm{mon}}\left(t_{2,i}\right) \cdot \left(\cos\vartheta_{2,i} - \cos\vartheta_{2,i+1}\right) \cdot \frac{\sum_{j=1}^{n_2} \Delta\varphi_{1,j} \cdot \left(c_{\mathrm{FH}} \cdot F_{2,i,j} - c_{\mathrm{FD}} \cdot f_{2,0}\right)}{s_2 \cdot w_{2,f} \cdot R_{2,g}} \end{array} \right) \quad (24)$$

Only the more important contributions to the combined measurement uncertainty are listed in table 2.

Table 2. Uncertainty budget

Quantity	Symbol	Value	Uncertainty	Unit	Sensitivity	Contribution/ lm	Relative contribution
Luminous responsivity 1	s_1	3.065E-10	9.195E-13	A lx^{-1}	1.88E+12	1.73	0.00150
Luminous responsivity 2	s_2	4.111E-10	1.2333E-12	A lx^{-1}	1.43E+12	1.77	0.00153
Spectral matching exponent 1	$m_{1,y}$	0.021	0.015	1	20	0.30	0.00026
Spectral matching exponent 2	$m_{2,y}$	0.036	0.015	1	18	0.27	0.00023
CCT or distribution temperature	T	2762	10	K	0.012	0.12	0.00011
Uncertainty in r	Δr	0.000	0.0020	m	901	1.80	0.00156
Calibration factor for frequency F	c_{FH}	1.000	0.0005	1	1141	0.57	0.00049
Calibration factor for frequency f	c_{FD}	1.000	0.0050	1	10.4	0.05	0.00005
Voltage to frequency converter 1	$w_{1,f}$	50084.9	25	Hz V^{-1}	0.012	0.31	0.00027
Voltage to frequency converter 2	$w_{2,f}$	50056.1	25	Hz V^{-1}	0.0118	0.29	0.00026
Amplification gain 1	$R_{1,g}$	1.000E+09	99996	Ω	6.223E-07	0.06	0.00005
Amplification gain 2	$R_{2,g}$	9.997E+08	99966	Ω	5.430E-07	0.05	0.00005
Calibration factor for c_{mon}	c_{cm}	1.000	0.0005	1	1162	0.58	0.00050
Correction factor for stray light	c_{str}	0.9995	0.0005	1	1134	0.57	0.00049
Luminous flux	Φ	**1154.1**				**3.27**	**0.0028**

Thus the expanded $k = 2$ measurement uncertainty will be 0.56 % at the moment. That is nearly the same as we reached with the large gimbal mounted system. We must keep in mind that the very high flexibility of this new goniophotometer complicates the position determination of the photometer. However, in future a position look-up-table is planned to minimize the radius uncertainty. An on-line-laser-tracer system to measure the photometer's position is also possible.

Meanwhile the robot goniophotometer is sufficiently characterised to be used for all traditional (illuminance based) calibrations and even an international RMO-comparison which is in progress. This capability complies with the listed requirements (15 to 17).

The next step at PTB uses the "basic concept of the robot goniophotometer" with imaging luminance meters replacing the "traditional photometers" to operate the system as "Near-Field-Goniophotometer" allowing the direct traceability of measured luminance distributions to maintained photometric units. This future step will comply with the last point (18) in our list of requirements.

3 Conclusion

The history of goniophotometry at PTB over more than 50 years is presented. Beginning with a manually operated single lever system with visual photometer via different gimbal mounted goniophotometers up to a state of the art robot goniophotometer for the 21st century. The latter has the potential to operate in "traditional" and in "near field" mode over many years. This will solve the upcoming demands for traceability of photometric units for instant from solid state lighting technology.

References

1 OHNO, Y. 1995. *Realization of NIST Luminous Flux Scale Using an Integrating Sphere with an External Source*. CIE Proceedings, 23rd Session New Delhi

2 SEWIG, R. 1938. *Handbuch der Lichttechnik*, Band 1, Pages 319 and 321, Berlin, Springer Verlag

3 FÖRSTE, D. 1966. *Zur Lichtstrommessung an Lampen mit ungleichmäßiger Lichtverteilung*, PTB-Mitteilungen, 1/66, pages 18 to 20, Braunschweig, PTB

4 FÖRSTE, D. 1979. *Ein Goniophotometer zur genauen Bestimmung des Lichtstroms*, Licht-Forschung, 1. Jahrgang, 3/79, pages 30 to 36, Heidelberg, Hüthig Verlag

5 FÖRSTE, D. 1980. *Elimination des Fremdlichts bei der Lichtstrombestimmung mit dem Goniophotometer*, Licht-Forschung, 2. Jahrgang, 1/80, pages 27 to 29, Heidelberg, Hüthig Verlag

6 ERB, W. 1997. *PTB Network for realization and maintenance of the candela*, Metrologia, 34/97, pages 115 to 124, Bristol, UK

7 SAUTER, G. 1996. *Kalibrierung von Lichtstärke-Normallampen und Angabe der Messunsicherheit*, PTB interner Bericht, Braunschweig, PTB

8 SAUTER, G. 1996. *Goniophotometry: new calibration method and instrument design*, Metrologia, **32** (1995/96), pages 685 to 688, Bristol, UK

9 http://en.wikipedia.org/wiki/Denavit-Hartenberg_Parameters

10 LINDEMANN, M. 2009. *Photometry and Colorimetry of Reference LEDs by Using a Compact Goniophotometer*, MAPAN – Journal of Metrology Society of India, Vol. 24, No 3, pages 143-152, New Delhi, India

11 BIZJAK, G. 2009. *Determination of Stray Light at the PTB Goniophotometer Facility*, MAPAN – Journal of Metrology Society of India, Vol. 24, No 3, pages 163-173, New Delhi, India